Methods

Yeast two-hybrid system. The two-hybrid screen, mating experiments, and X-gal colony filter assay were performed as described[19].

***In vitro* binding of p38 and MEF2C.** Glutathione-agarose beads bound with a GST fusion protein of wtp38 (GST–wtp38) were incubated with different amounts of MEF2C in buffer A (10 mM Tris-HCl, pH 7.9, 250 mM NaCl, 25 mM imidazole and 0.05% Triton-X-100) containing 2% BSA with or without cold ATP (20 μM) for 3 h after blocking the nonspecific binding with 2% BSA in buffer A for 3 h. After the beads were washed 6 times with buffer A, they were subjected to SDS–PAGE followed by transfer to nictocellulose; His–MEF2C was detected using Ni-NTA conjugated with alkaline phosphatase (Qiagen), and GST–p38 was detected with rabbit anti-p38 antibody together with peroxidase coupled to sheep anti-rabbit IgG (Cappel).

***In vitro* kinase assays.** Equal amounts (2 μg) of His–MEF2C, GST–c-Jun (residues 1–93)[3] or MBP (Sigma) were used as substrates. His-tagged wtp38 (ref. 4), His-tagged ERK2 (ref. 25) or flag-tagged JNK1 (ref. 3) were used as kinases. The kinase reaction and quantification were performed as described[3,26].

EMSA. Nuclear extracts of RAW 264.7 cells treated with or without LPS (10 ng ml^{-1}) for different times were incubated with a double-stranded, ^{32}P-labelled oligonucleotide containing a MEF2 binding site as a probe[11]. An unlabelled MEF2 oligonucleotide probe and an oligonucleotide with a mutation in the MEF2 site (MEF2mut)[11] were used as competitors to determine the binding specificity.

Reporter gene assays. THP-1 cells were transfected with DEAE-Dextran[22] and RAW 264.7 cells with calcium phosphate[27]. Cells were transfected with a β-galactosidase expression vector pCMV-β, with the reporter plasmid pG5E1-bLuc, with an expression vector encoding a GAL4–MEF2C fusion protein or GAL4(1–147) or GAL4–MEF2C mutants, and with the expression vector encoding a constitutively active form of MKK6b(E) or with empty vector pcDNA3. In some experiments the cells were also transfected with increasing amounts of DNA (0, 2, 4, 8, 12 or 16 μg) from an expression plasmid for p38(M). The total amount of DNA for each transfection was kept constant using pcDNA3. In studies using FHPI, the inhibitor was added (3 μM) 36 h after transfection for 1 h; and the cells were then treated with or without LPS for 8 h. LPS (5 μg ml^{-1} and 10 ng ml^{-1}) was used to stimulate THP-1 and RAW 264.7 cells, respectively. The relative luciferase activities presented were normalized by dividing the luciferase activity by β-galactosidase activity.

Phosphoamino-acid analysis and phosphopeptide mapping. These methods were performed as described[18]. GAL4–MEF2C fusion protein and mutants from [^{32}P]orthophosphate-labelled permanently transfected RAW 264.7 cells (1 mCi ml^{-1}, 2 h) treated with or without LPS (10 ng ml^{-1}, 2 h) were immunoprecipitated with anti-GAL4 DNA-binding domain monoclonal antibody RK5C1 (Santa Cruz).

Received 18 November 1996; accepted 21 January 1997.

1. Morrison, D. C. *et al.* Bacterial endotoxins and pathogenesis of Gram-negative infections: current status and future direction. *J. Endotoxin Res.* 1, 71–83 (1994).
2. Blumer, K. J. & Johnson, G. L. Diversity in function and regulation of MAP kinase pathways. *Trends Biochem. Sci.* 19, 236–240 (1994).
3. Derijard, B. *et al.* JNK1: A protein kinase stimulated by UV light and Ha-Ras that binds and phosphorylates the c-Jun activation domain. *Cell* 76, 1025–1037 (1994).
4. Han, J., Lee, J.-D., Bibbs, L. & Ulevitch, R. J. A MAP kinase targeted by endotoxin and hyperosmolarity in mammalian cells. *Science* 265, 808–811 (1994).
5. Zhou, G., Bao, Z. Q. & Dixon, J. E. Components of a new human protein kinase signal transduction pathway. *J. Biol. Chem.* 270, 12665–12669 (1995).
6. Lee, J.-D., Ulevitch, R. J. & Han, J. Primary structure of BMK1: A new mammalian MAP kinase. *Biochem. Biophys. Res. Commun.* 213, 715–724 (1995).
7. Lee, J. C. *et al.* Identification and characterization of a novel protein kinase involved in the regulation of inflammatory cytokine biosynthesis. *Nature* 372, 739–746 (1994).
8. Raingeaud, J. *et al.* Pro-inflammatory cytokines and environmental stress cause p38 MAP kinase activation by dual phosphorylation on tyrosine and threonine. *J. Biol. Chem.* 270, 7420–7426 (1995).
9. Beyaert, R. *et al.* The p38/RK mitogen-activated protein kinase pathway regulates interleukin-6 synthesis in response to tumour necrosis factor. *EMBO J.* 15, 1914–1923 (1996).
10. Martin, J. F., Schwarz, J. J. & Olson, E. N. Myocyte enhancer factor (MEF) 2C: A tissue-restricted member of the MEF-2 family of transcription factors. *Proc. Natl Acad. Sci. USA* 90, 5282–5286 (1993).
11. McDermott, J. C. *et al.* hMED2C gene encodes skeletal muscle- and brain-specific transcription factors. *Mol. Cell. Biol.* 13, 2564–2577 (1994).
12. Leifer, D. *et al. Proc. Natl Acad. Sci. USA* 90, 11546–1550 (1993).
13. Durfee, T. *et al.* The retinoblastoma protein associates with the protein phosphatase type 1 catalytic subunit. *Genes Dev.* 7, 555–569 (1993).
14. Martin, J. F. *et al.* A *Mef2* gene that generates a muscle-specific isoform via alternative mRNA splicing. *Mol. Cell. Biol.* 14, 1647–1656 (1994).
15. Molkentin, J. D., Black, B. L., Martin, J. F. & Olson, E. N. Mutational analysis of the DNA binding, dimerization, and transcriptional activation domains of MEF2C. *Mol. Cell. Biol.* 16, 2627–2636 (1996).
16. Jiang, Y. *et al.* Characterization of the structure and function of a new mitogen-activate protein kinase (p38β). *J. Biol. Chem.* 271, 17920–17926 (1996).
17. Wang, H.-C. & Erikson, R. L. Activation of protein serine/threonine kinases p42, p43, and p87 in Rous sarcoma virus-transformed cells: Signal transduction/transformation-dependent MBP kinases. *Mol. Biol. Cell* 3, 1329–1337 (1992).
18. Boyle, W. J., VanDerGrve, P. & Hunter, T. Phosphopeptide mapping and phosphoamino acid analysis by two dimensional separation on thin-layer cellulose plates. *Methods Enzymol.* 201, 110–148 (1991).
19. Han, T.-H. & Prywes, R. Regulatory role of MEF2D in serum induction of the c-jun promoter. *Mol. Cell. Biol.* 15, 2907–2915 (1995).
20. Newell, C. L., Deisseroth, A. B. & Lopes-Berestein, G. Interaction of nuclear proteins with an AP-1/CRE-like promoter sequence in the human TNF-alpha gene. *J. Leukocyte Biol.* 56, 27–35 (1994).
21. Shin, H. S. *et al.* Definition of a lipopolysaccharide-responsive element in the 5'-flanking regions of MuRantes and crg-2. *Mol. Cell. Biol.* (1996). (Author: Volume? Pages?)
22. Mackman, N., Brand, K. & Edgington, T. S. Lipopolysaccharide-mediated transcriptional activation of the human tissue factor gene in THP-1 monocytic cells requires both activator protein 1 and nuclear factor kappa B binding sites. *J. Exp. Med.* 174, 1517–1526 (1991).
23. Fujihara, M., Muroi, M., Muroi, Y., Ito, N. & Suzuki, T. Mechanism of lipopolysaccharide-triggered junB activation in a mouse macrophage-like cell line (J774). *J. Biol. Chem.* 268, 14898–14905 (1993).
24. Hambleton, J., Weinstein, S. L., Lem, L. & DePranco, A. L. Activation of c-Jun N-terminal kinase in bacterial lipopolysaccharide-stimulated macrophages. *Proc. Natl Acad. Sci. USA* 93, 2774–2778 (1996).
25. Robbins, D. J. *et al.* Regulation and properties of extracellular signal-regulated protein kinases 1 and 2 in vitro. *J. Biol. Chem.* 268, 5097–5106 (1993).
26. Han, J. *et al.* Characterization of the structure and function of a novel MAP kinase kinase (MKK6). *J. Biol. Chem.* 271, 2886–2891 (1996).
27. Han, J., Brown, T. & Beutler, B. Endotoxin-responsive sequences control cachectin/tumo necrosis factor biosynthesis at the translational level. *J. Exp. Med.* 171, 465–475 (1990).

Acknowledgements. We thank L. Wu for the help with two-hybrid screening; R. J. Davis for JNK1 cDNA; M. Karin for GST-c-Jun (1–93) expression plasmid; R. Prywes for pJluc and pJSXluc reporter constructs; and B. Chastain for secretarial assistance. This work was supported by grants from the National Institutes of Health, and the American Heart Association. J. Han is an established investigator of the American Heart Association.

Correspondence and requests for materials should be addressed to J. H. (e-mail: jhan@scripps.edu).

Direct observation of the rotation of F_1-ATPase

Hiroyuki Noji*, Ryohei Yasuda†, Masasuke Yoshida* & Kazuhiko Kinosita Jr†

* *Research Laboratory of Resources Utilization, Tokyo Institute of Technology, Nagatsuta 4259, Midori-ku, Yokohama 226, Japan*
† *Department of Physics, Faculty of Science and Technology, Keio University, Hiyoshi 3-14-1, Kohoku-ku, Yokohama 223, Japan*

Cells employ a variety of linear motors, such as myosin[1–3], kinesin[4] and RNA polymerase[5], which move along and exert force on a filamentous structure. But only one rotary motor has been investigated in detail, the bacterial flagellum[6] (a complex of about 100 protein molecules[7]). We now show that a single molecule of F_1-ATPase acts as a rotary motor, the smallest known, by direct observation of its motion. A central rotor of radius ~1 nm, formed by its γ-subunit, turns in a stator barrel of radius ~5 nm formed by three α- and three β-subunits[8]. F_1-ATPase, together with the membrane-embedded proton-conducting unit F_0, forms the H^+-ATP synthase that reversibly couples transmembrane proton flow to ATP synthesis/hydrolysis in respiring and photosynthetic cells[9,10]. It has been suggested that the γ-subunit of F_1-ATPase rotates within the αβ-hexamer[11], a conjecture supported by structural[8], biochemical[12,13] and spectroscopic[14] studies. We attached a fluorescent actin filament to the γ-subunit as a marker, which enabled us to observe this motion directly. In the presence of ATP, the filament rotated for more than 100 revolutions in an anticlockwise direction when viewed from the 'membrane' side. The rotary torque produced reached more than 40 pN nm^{-1} under high load.

In the crystal structure of mitochondrial F_1-ATPase[8], rigid[15] coiled-coil α-helices of the γ-subunit penetrate the central cavity of the $\alpha_3\beta_3$ and extend into the stalk region that links F_1-ATPase to the F_0 portion. The amino terminus of the β-subunits is on the side opposite the stalk region of the γ-subunit. To fix the $\alpha_3\beta_3\gamma$ subcomplex on a glass plate, the subcomplex derived from a thermophilic bacterium was expressed in *Escherichia coli*, with ten histidines (His tag) linked to the N terminus of each β-subunit. The

glass plate was coated with horseradish peroxidase conjugated with Ni^{2+}-nitrilotriacetic acid (Ni-NTA), which has a high affinity for a His-tag and thus bound the subcomplex through the three β-subunits, with the F_0 side ('membrane' side) away from the glass (Fig. 1a). To visualize the rotation, γ-Ser107, which is presumably in the stalk region of the γ-subunit[8], was replaced with cysteine, and α-Cys193, the only cysteine in the wild-type $\alpha_3\beta_3\gamma$ subcomplex, was replaced with serine by site-directed mutagenesis[16]; the introduced cysteine was biotinylated. A fluorescently labelled, biotinylated actin filament was attached to the γ-subunit through streptavidin, which has four binding sites for biotin.

Rotating actin filaments were found in the field of an epifluorescence microscope when 2 mM ATP was infused into a flow chamber containing actin-tagged $\alpha_3\beta_3\gamma$ subcomplexes on the bottom plate (Fig. 2). On average, one out of 70 filaments rotated continuously in one direction. Fifteen out of 70 showed only irregular to-and-fro fluctuation around one fixed point; these were observed for at least 25 s, because fluctuating filaments in some cases started to rotate. Others were immobile, being attached to the glass surface at two or more points. Most of the rotating filaments had their rotation axis at one end of the filament (Fig. 2a), whereas some had the axis at the middle and rotated like a propeller (Fig. 2b). As the $\alpha_3\beta_3\gamma$ subcomplex was fixed to the glass plate through (presumably) three β-subunits and the actin filament was attached to the γ-subunit, this result shows that the γ-subunit rotates in the centre of the $\alpha_3\beta_3$ cylinder (Fig. 1a). The other subunits, δ and ε, are not necessary for the rotation; they may be a part of the stator and rotor, respectively[17].

The time course of rotation of individual actin filaments is shown in Fig. 3. It is clear that the filaments rotate only in one direction. We observed 90 rotating filaments altogether and all, without exception, rotated anticlockwise when viewed from the membrane side (Fig. 1a). In the crystal structure[8], the anticlockwise rotation of the central γ-subunit allows it to interact sequentially with the three

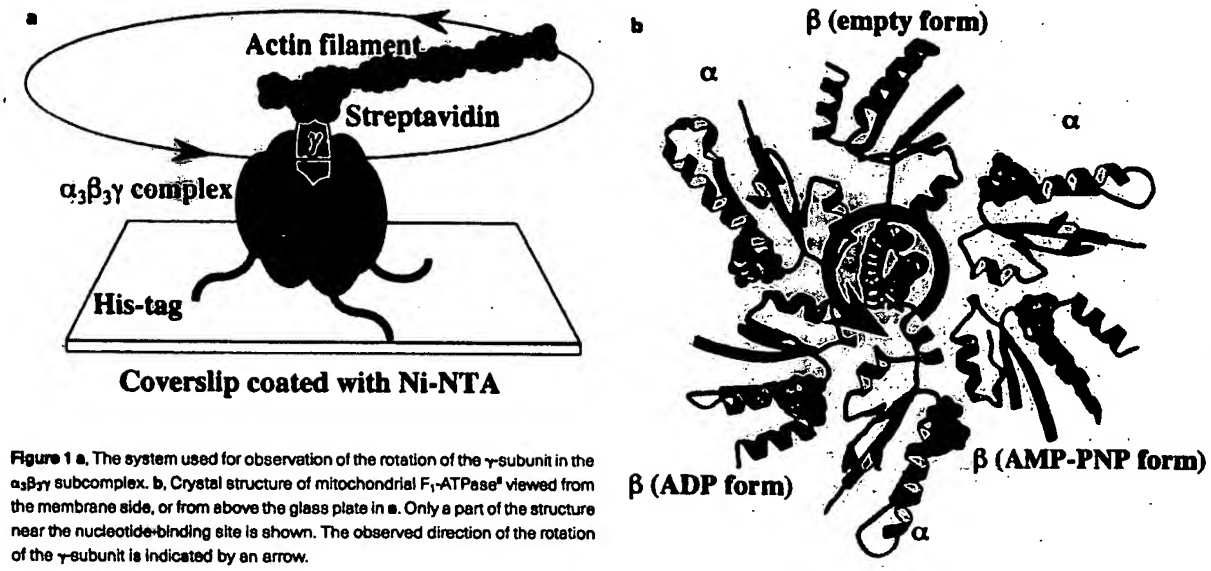

Figure 1 a, The system used for observation of the rotation of the γ-subunit in the $\alpha_3\beta_3\gamma$ subcomplex. b, Crystal structure of mitochondrial F_1-ATPase[8] viewed from the membrane side, or from above the glass plate in a. Only a part of the structure near the nucleotide-binding site is shown. The observed direction of the rotation of the γ-subunit is indicated by an arrow.

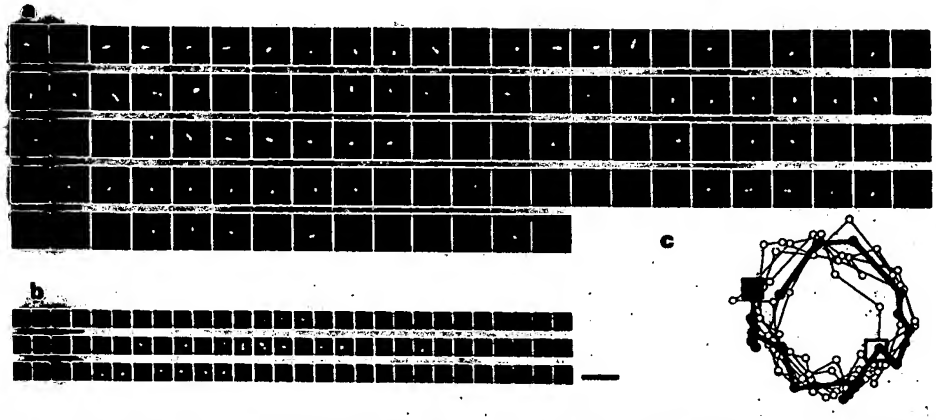

Figure 2 Sequential images of a rotating actin filament attached to the γ-subunit in the $\alpha_3\beta_3\gamma$ subcomplex. In the inverted microscope, the specimen is viewed from the bottom and its mirror image is formed on the camera[22]. Therefore, images shown here correspond to the view from the top (Fig. 1a). a, A rotating filament with the rotation axis at one edge. Length from the axis to tip, 2.6 μm; rotary rate, 0.5 r.p.s.; time interval between images, 133 ms. b, A rotating filament with the rotation axis at the middle of the filament. Total length of the filament, 2.4 μm; rotary rate, 1.3 r.p.s.; time interval between images, 33 ms. Scale bar, 5 μm in a and b. c, A trace of the centroid of the filament image in a. The trace starts at the filled square and ends at the open square. The first revolution is shown in the thick line.

forms of the β-subunits in the order: empty form, ADP-bound form, AMP-PNP (an ATP analogue)-bound form (Fig. 1b). This sequence is equivalent to the catalytic transition in one β-subunit in the order: ATP → ADP → empty forms, the order expected in the ATP hydrolysis reaction.

Figure 2 shows that the rotary speed was not constant and that even small, momentary reversals occurred occasionally. The fluctuation should in part be of brownian origin, but a certain angle-dependence was also noticeable (in Fig. 2a, for example, the filament tends to dwell in the bottom half, as in Fig. 2c). In filaments with lower average speeds, frequent pauses, accompanied by fluctuation, were observed (Fig. 3), often at the same angle(s). Obstruction by nearby proteins is a likely explanation, but intrinsic properties of this rotary motor may also contribute to these angle-dependent irregularities. In some cases, the angular distribution appeared to have three peaks separated by 120°, but precise analysis was hampered by the brownian fluctuation. Observation was terminated after a pause of >30 s or when the filament became completely immobile (39 out of the 90 cases), or when the filament was torn off near the attachment point and floated into solution (7/90), or after rotation continued for >1 min (44/90). Some filaments continued to rotate for >10 min.

When ATP was absent, there was no rotary motion apart from the brownian fluctuation ('−ATP' in Fig. 3), which, on rare occasions, accumulated over several minutes into a few turns in either direction. Azide, an inhibitor of the ATPase activity of F_1-ATPase and of the $\alpha_3\beta_3\gamma$ subcomplex[18], blocked rotation in the presence of ATP ('+ATP + NaN_3' in Fig. 3). Because rotation was rare, we did an 'unpredicted test' in which we observed 1,800 filaments under each of the '+ATP', '−ATP' or '+ATP + NaN_3' conditions without knowing the identity of the sample. We made a complete search on 15 chambers, taking ~30 min for each chamber and stopping for 25 s at every actin filament that showed some sign of movement. We found that 25 filaments in '+ATP' made >5 turns during the first 25 s of observation. No filaments made >2 turns in 25 s under the '−ATP' or '+ATP + NaN_3' conditions.

The stoichiometry of three ATPase catalytic sites (on β-subunits) per single γ-subunit in the F_1-ATPase indicates a rotary rate (without load) of 17 revolutions per second (r.p.s.), if the fixed subcomplex hydrolysed ATP at the same rate as was measured in solution (52 ATP per second). The observed rate of filament rotation, on the other hand, was at most ~4 r.p.s. and lower for longer filaments (Fig. 3), suggesting that the γ-subunit carrying an actin filament rotated against a heavy load produced by hydrodynamic friction on the filament. Indeed, the torque needed to rotate an actin filament at the observed speed is quite large, >45 pN nm for the filament in Fig. 2a and >23 pN nm for Fig. 2b (see Methods). If this torque is produced at the β–γ interface at the radius of ~1 nm from the central axis of the $\alpha_3\beta_3$ cylinder[8], the force that makes the γ-subunit slide past the β-subunit would amount to >45 pN (Fig. 2a) or >23 pN (Fig. 2b). By comparison, individual linear motors produce a sliding force of 3–6 pN (myosin[1–3]), 5 pN (kinesin[4]), or 14 pN (RNA polymerase[5]). The slower movement under higher load is a feature common to all known linear motors and the flagellar motor. Whether the coupling between ATP hydrolysis and the rotation in F_1-ATPase is loose[19] as in linear motors, or as tight as in the flagellar motor[20], remains to be investigated.

Taken together, this work provides discriminating evidence for the physical unidirectional rotation of the γ-subunit in the F_1-ATPase. It is now clear that the γ-subunit constitutes the rotating 'shaft' that mediates the energy exchange between the proton flow at F_0 and ATP synthesis/hydrolysis at F_1-ATPase. Taking advantage of the single molecule observation system, we plan to analyse the torque and speed, mechanism of force generation, effect of ATP concentration, efficiency and architecture of the rotor and stator of this new type of enzyme, the smallest biological rotary motor known. □

Methods

Materials. The mutant (α-C193S, γ-S107C) $\alpha_3\beta_3\gamma$ subcomplex of thermophilic *Bacillus* PS3 was purified as described[21]. The subcomplex was treated with a 2–10 molar excess of 6-{*N*'-[2-(*N*-maleimido)ethyl]-*N*-piperazinyl-amido}hexyl-D-biotinamide (biotin-PEAC$_5$-maleimide, Dojindo) in 20 mM 3-[*N*-morpholino]propanesulphonic acid-KOH (MOPS-KOH, pH 7.0) and 100 mM KCl for 6 h on ice. Specific biotinylation of the γ-subunit was confirmed by western blotting with horseradish peroxidase avidin D (Vector Labs). Catalytic activities were measured at 25 °C at pH 7.0 in the presence of 50 mM KCl; the mutant subcomplex hydrolysed 52 ATP molecules per second,

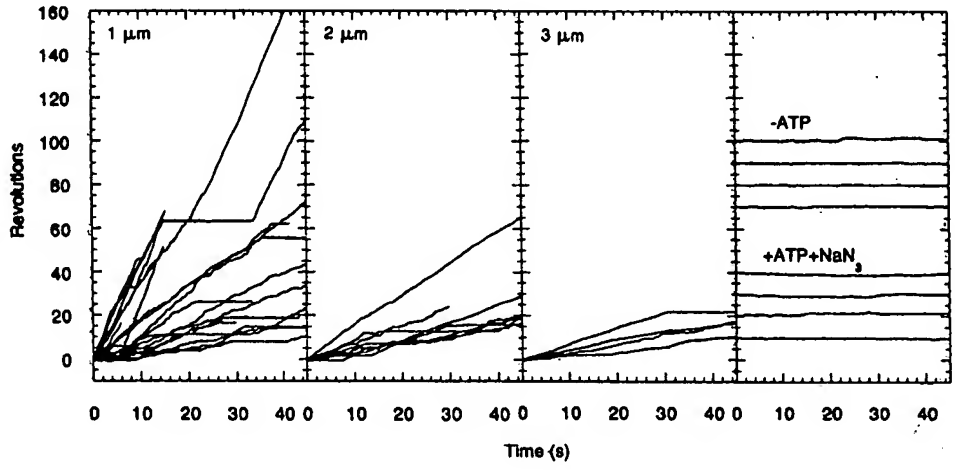

Figure 3 Time course of the rotation of the γ-subunit; each line represents one filament. The ordinate represents the number of anticlockwise revolutions. Rotating filaments, all in the presence of 2 mM ATP, are classified into three groups according to their length ('1 μm' indicates 0.5–1.4 μm; '2 μm', 1.5–2.4 μm; '3 μm', 2.5–3.4 μm). Only those filaments that rotated around one end are shown, for which the rotating angles were conveniently estimated by centroid analysis as in Fig. 2c. The angular resolution in these plots is estimated to be ~20°, or worse in some cases, because the filament was not always straight and part of the filament occasionally went out of focus. '−ATP', without ATP; '+ATP + NaN_3', in the presence of 2 mM ATP and 10 mM NaN_3; for these control experiments, those filaments that moved most are selected and shown.

the wild-type subcomplex 52 ATP s^{-1}, and the native F_1-ATPase 39 ATP s^{-1}. Rabbit skeletal actin (30 μM) was incubated with 150 μM biotin-$PEAC_5$-maleimide in 100 mM KCl, 1 mM $MgCl_2$, 10 mM MOPS-KOH (pH 7.0) and 0.3 mM NaN_3 at room temperature for 2 h. The actin was depolymerized in 2 mM MOPS-KOH (pH 7.0), 0.2 mM $CaCl_2$ and 2 mM ATP. Residual biotin was removed on a Sephadex G-25 column. Biotinylated actin (5 μM) was polymerized in 10 mM 2-(cyclohexylamino)ethanesulphonic acid-KOH (pH 8.8), 100 mM KCl, 1 mM $MgCl_2$ and 5 μM phalloidin–tetramethylrhodamine B isothiocyanate conjugate (Fluka) overnight at 4 °C, and crosslinked with 500 μM disuccinimidyl suberate (Pierce) at room temperature for 2 h. The reaction was quenched with 50 mM Tris-HCl (pH 8.8).

Immobilization of proteins. A flow cell for microscopic observation was constructed from a bottom coverslip (24 × 36 mm^2; Matsunami) coated with nitrocellulose and a top coverslip (18 × 18 mm^2), separated by two greased strips of Parafilm cover sheet. 0.6–1.2 μM of horseradish peroxidase-conjugated Ni-NTA (Qiagen) was introduced into the flow cell and allowed to adhere to the glass surface for 2 min. The cell was washed with buffer A (10 mg ml^{-1} BSA, 10 mM MOPS-KOH (pH 7.0), 50 mM KCl, 4 mM $MgCl_2$). Infusion and washing were repeated as follows: infusion of 10–100 nM biotinylated $\alpha_3\beta_3\gamma$ subcomplex in buffer A (5 min), washing with buffer A, infusion of 180 nM streptavidin (Sigma) in buffer A (2 min), washing with buffer A, and infusion of 100 nM biotinylated fluorescent actin filaments in buffer A (5–15 min). The last wash was carried out with 0.5% 2-mercaptoethanol and an oxygen-scavenger system[22] in buffer A containing, where indicated, 2 mM ATP or 10 mM NaN_3. Observation started within 1 min of the beginning of the last washing. The actin filaments did not bind to the glass plate without the biotinylated subcomplexes. Also, the binding was dependent on streptavidin. In a control experiment, His-tagged subcomplexes fluorescently labelled at γ-Cys107 were fixed on a Ni-NTA surface and extensively washed with buffer A; subsequent washings with buffer A containing 50 mM imidazole (pH 7.4) removed >85% of the fluorescence. These results ensure that the actin filaments were attached to the biotinylated $\alpha_3\beta_3\gamma$ subcomplexes which were fixed to the glass surface through the histidine tags.

Observation of rotation. Actin filaments were observed under an epifluorescence microscope (Diaphot TMD, Nikon) with excitation and emission wavelengths at 546 nm and 560–620 nm, respectively. Images were taken with a CCD camera (Dage MTI) attached to an image intensifier (KS-1381, Videoscope), recorded on an 8-mm video tape, and analysed with a digital image processor (DIPS-C2000, Hamamatsu Photonics)[2,23]. The frictional torque for the propeller rotation is given[24], in the simplest approximation, by $(\pi/3)\omega\eta L^3/[\ln(L/2r) - 0.447]$, where ω is the angular velocity, η (10^{-3} N s m^{-2}) the viscosity of the medium, L the length of actin filament, and r (5 nm) the radius of the filament. For the rotation around one end of the filament, the torque is four times the above value. These values are actually underestimated, because the viscous drag near the glass surface is higher (up to ~3-fold[24] if all of the filament lies at a height of (5 + 8) nm from the glass surface, 5 nm being the filament radius and 8 nm the height[8] of $\alpha_3\beta_3$) and because possible contact with the surface would produce additional friction.

Received 11 November 1996; accepted 7 January 1997.

1. Finer, J. T., Simmons, R. M. & Spudich, J. A. *Nature* 368, 113–119 (1994).
2. Miyata, H. *et al. Biophys. J.* 68, 286S–290S (1995).
3. Ishijima, A. *et al. Biochem. Biophys. Res. Commun.* 199, 1057–1063 (1995).
4. Svoboda, K., Schmidt, C. F., Schnapp, B. J. & Block, S. M. *Nature* 365, 721–727 (1993).
5. Yin, H. *et al. Science* 270, 1653–1657 (1995).
6. Berg, H. C. & Anderson, R. A. *Nature* 245, 380–382 (1973).
7. Aizawa, S. & Jones, C. J. *Adv. Microb. Physiol.* 32, 110–172 (1991).
8. Abrahams, J. P., Leslie, A. G. W., Lutter, R. & Walker, J. E. *Nature* 370, 621–628 (1994).
9. Mitchell, P. *Nature* 191, 144–148 (1961).
10. Kagawa, Y. & Racker, E. *J. Biol. Chem* 241, 2467–2474 (1966).
11. Boyer, P. D. *Biochim. Biophys. Acta* 1140, 215–250 (1993).
12. Duncan, T. M., Bulygin, V. V., Zhou, Y., Hutcheon, M. L. & Cross, R. L. *Proc. Natl Acad. Sci. USA* 92, 10964–10968 (1995).
13. Zhou, Y., Duncan, T. M., Bulygin, V. V., Hutcheon, M. L. & Cross, R. L. *Biochim. Biophys. Acta* 1275, 96–100 (1996).
14. Sabert, D., Engelbrecht, S. & Junge, W. *Nature* 381, 623–625 (1996).
15. Noji, H., Amano, T. & Yoshida, M. *J. Bioenerg. Biomemb.* 28, 451–457 (1996).
16. Kunkel, T. A., Bebenek, K. & McClary, J. *Meth. Enzymol.* 204, 125–139 (1991).
17. Aggeler, R. & Capaldi, R. A. *J. Biol. Chem.* 271, 13888–13891 (1996).
18. Yoshida, M., Sone, N., Hirata, H. & Kagawa, Y. *J. Biol. Chem.* 252, 3480–3485 (1977).
19. Oosawa, F. & Hayashi, S. *Adv. Biophys.* 22, 151–183 (1986).
20. Meister, M., Lowe, G. & Berg, H. C. *Cell* 49, 643–650 (1987).
21. Matsui, T. & Yoshida, M. *Biochim. Biophys. Acta* 1231, 139–146 (1995).
22. Harada, Y., Sakurada, K., Aoki, T., Thomas, D. D. & Yanagida, T. *J. Mol. Biol.* 216, 49–68 (1990).
23. Sase, I., Miyata, H., Corrie, J. E. T., Craik, J. S. & Kinosita Jr, K. *Biophys. J.* 69, 323–328 (1995).
24. Hunt, A. J., Gittes, F. & Howard, J. *Biophys. J.* 67, 766–781 (1994).

Acknowledgements. H.N. and R.Y. contributed equally to this work. We thank T. Hisabori, R. Muneyuki, T. Amano and G. Marriott for critically reading the manuscript; H. Itoh and M. Hosoda (Hamamatsu Photonics) for image processing; T. Matsui for constructing subcomplex expression system; and F. Motojima for producing Fig. 1b. This work was supported in part by Grants-in-Aid from Ministry of Education, Science, Sports and Culture in Japan (M.Y., K.K.), and a Keio University Special Grant-in-Aid (K.K.). R.Y. is a Research Fellow of the JSPS.

Correspondence and requests for materials should be addressed to M.Y. (e-mail: myoshida@rea.titech.ac.jp).

erratum

Spatio-temporal frequency domains and their relation to cytochrome oxidase staining in cat visual cortex

Doron Shoham, Mark Hübener, Silke Schulze, Amiram Grinvald & Tobias Bonhoeffer

Nature 385, 529–533 (1997)

In this Letter, an editing error in the *Nature* office led to a misleading first sentence in the last paragraph. The complete paragraph should read as follows:

Tracing studies have shown that blobs in cat visual cortex are specifically connected to other visual cortical areas[29,30] and that they receive a strong input from Y-cells in the lateral geniculate nucleus[11]. Furthermore, we have preliminary evidence that low spatial frequency domains, like blobs, receive a stronger input from geniculate Y-cells[31], which would be consistent with the preference for low spatial and high temporal frequencies revealed here. The blob and interblob regions of cat visual cortex, like their counterparts in primate visual cortex, appear to be compartments of parallel pathways that are specialized for analysing different attributes of the visual scene. □

correction

Transmission dynamics and epidemiology of BSE in British cattle

R. M. Anderson, C. A. Donnelly, N. M. Ferguson, M. E. J. Woolhouse, C. J. Watt, H. J. Udy, S. MaWhinney, S. P. Dunstan, T. R. E. Southwood, J. W. Wilesmith, J. B. M. Ryan, L. J. Hoinville, J. E. Hillerton, A. R. Austin & G. A. H. Wells

Nature 382, 779–788 (1996).

In Table 2 of this Letter, the reported number of cases saved for policy 9 was erroneously given for 1996 to 2001 rather than for 1997 to 2001. The number should be 584 rather than 797. Thus, the number of cases saved in policies 11–14 should be reduced by 213. Also, the culling policy description for policy 6 should begin 'As 5)' rather than 'As 15)'.

An error caused Figs 1d and e in this article to be transposed. The legends are correct.

On page 783, in the first column in the sixth line of text 'F and G are two operators' should have been 'G and F are two operators'.

Finally, the manuscript on maternal transmission of the BSE agent in cows by J. W. Wilesmith *et al.* described in the paper as ref. 6, under consideration by *Nature*, has been withdrawn. □